Temperature–Salinity Criterion for Inhibition of Deep Convection

DAN E. KELLEY

Oceanography Department, Dalhousie University, Halifax, Nova Scotia, Canada

22 November 1993 and 28 March 1994

ABSTRACT

Malmberg's salinity criterion for the inhibition of oceanic deep convection is extended here to account for increases in salinity caused by evaporation, brine rejection, and mixed-layer deepening. Roughly speaking, accounting for evaporation permits deep convection for waters up to ~0.2 psu fresher than Malmberg's critical salinity of 34.7 psu. An additional 0.2 psu of freshness is permitted in regions of ice formation at rates such as that in the Greenland Sea. Typically a further 0.1 psu is permitted because of the salinizing effect of mixed-layer deepening. On a global ocean scale, the difference between Malmberg's criterion and the present criterion is relatively minor: both criteria suggest that the North Atlantic is salty enough to feed the global thermohaline overturning cell but that the North Pacific is too fresh. On a regional scale, the difference between the criteria is more significant. This is illustrated with surface salinity maps for the Greenland Sea, a region known to produce bottom water for the overturning cell. Each criterion predicts that the relatively fresh inshore waters are not capable of deep convection but that the saltier offshore waters are. However, the new criterion places the onshore–offshore dividing line 100–200 km closer to Greenland than does Malmberg's criterion. A large geographical area lies between the two dividing lines and would thus be misjudged by Malmberg's criterion. Furthermore, the new stability boundary is shifted inshore by a distance equal to the offshore decay scale of the buoyancy flux associated with cold air outbreaks from the continent. In effect, then, the buoyancy fluxes driving the ocean convection are much larger than otherwise would have been predicted.

1. Introduction

A major difficulty in detecting slow variations in the ocean or atmospheric state, such as those anticipated to result from increased greenhouse warming, is the presence of short-term (e.g., decadal) variability in the relevant geophysical time series (Broecker 1975, 1992). Although the existence of decadal variations in the ocean state has been recognized for some time (Brewer et al. 1983; Schlosser et al. 1991; Read and Gould 1992; Levitus 1989, 1990), the present understanding of cause and effect is too limited to permit disentangling these processes from presumed longer timescale global climate change signals.

A suspected link between oceanic motions and the state of the climate, perhaps in the form of the "conveyor belt" model (Broecker 1991), motivates much of the present effort to couple atmospheric and oceanic climate models. The principle of a connection between hydrographic properties and the rate of thermohaline overturning in the North Atlantic has been well established; reviews by Rooth (1982), Broecker and Denton (1989), and Weaver and Hughes (1992) provide an introduction to a growing literature. Accumulating evidence suggests that changes in hydrography are linked to changes in overturning rate. A surface freshening caused by the input of glacial meltwater during the termination of the last glaciation appears to have inhibited convection in the North Atlantic (Boyle 1990; Keigwin et al. 1991), causing large changes in European climate (Broecker 1991). Simulating this dramatic "Younger Dryas" event has become a litmus test for paleoclimate models (e.g., Wright and Stocker 1994). On shorter timescales, it has been speculated that decadal climate variations result from modulation of the rate of deep convection (Marsden et al. 1991; Mysak et al. 1990). Here again, changes in the surface hydrography are thought to be a key feedback link.

While numerical modeling is a powerful tool for exploring the *detailed* links between hydrography and convection in specific situations (Hakkinen et al. 1992; Madec et al. 1991a; Madec et al. 1991b; Skyllingstad et al. 1991), a simply stated principle underpins the *general* assumption of a link between hydrography and deep convection. The principle stems from Malmberg's (1969) suggestion that surface salinities less than a critical value of 34.7 psu will prevent local deep convection from producing water dense enough to drive the large-scale thermohaline overturning cell. The purpose of the present paper is to extend Malmberg's criterion (reviewed in section 2) to account for hydrographic changes associated with evaporation (section 3), brine rejection (section 4), and mixed-layer deepening (section 5). An application of the new

Corresponding author address: Dr. Dan E. Kelley, Dept. of Oceanography, Dalhousie University, Halifax, Nova Scotia B3H 4J1, Canada.

criterion to the North Atlantic and North Pacific is presented in section 6, and a summary is given in section 7.

2. Malmberg's salinity criterion

Malmberg's (1969) salinity criterion for inhibition of deep convection is illustrated schematically in Fig. 1. Two T–S curves are shown. The first is the T–S relationship for water at the freezing point; seawater cooled below this curve freezes and water in thermodynamic equilibrium with sea ice must have T–S properties lying on this curve. For typical ocean salinities, this curve is nearly independent of S, being approximated by the isotherm $T = -1.8\,^{\circ}\mathrm{C}$. The second curve is the T–S relationship for seawater with density equal to that of the deep water of the ocean basin, or of any other water mass whose convective renewal is of interest.

Consider two T–S values for near-surface water, labeled A and B in Fig. 1. If the water is cooled (in the absence of evaporation or freezing), then the T–S trajectories will follow the vertical arrows shown in the figure. For case A, surface waters will reach the freezing point before becoming as dense as the deep water. Leaving aside for the moment the issue of salinity increase accompanying ice formation, the insulating effect of the ice will prevent further densification of the surface waters, thus preventing renewal of the deep water. For case B, in contrast, the intersection of the cooling trajectory and the deep-water isopycnal is at a temperature exceeding the freezing point. Sustained cooling will thus increase the density to a value exceeding that of the deep water before the water parcel cools enough to freeze. Therefore, deep convection is possible, given sufficient cooling.

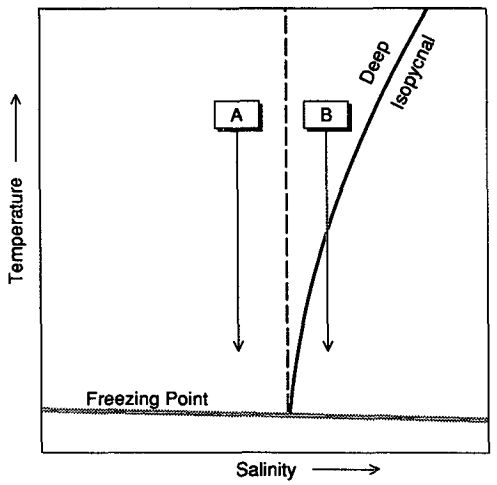

FIG. 1. Schematic T–S diagram used to explain Malmberg's (1969) salinity criterion for deep convection. The gray line along the bottom is the T–S relationship for seawater at the freezing point. The solid curve is the isopycnal T–S relationship for water types having density equal to that of the deep water. Points A and B are two hypothetical water masses, and the arrows extending from them represent their T–S evolution under the imposition of cooling in the absence of evaporation, brine rejection, or entrainment of different water masses. Malmberg's (1969) criterion states that cooling of waters whose T–S characteristics are to the right of the vertical dashed line (e.g., B) can result in deep convection, while waters to left (e.g., A) will freeze before getting dense enough to sink to the bottom.

Thus, Fig. 1 motivates a criterion that depends on salinity but not temperature. The critical value of the salinity, denoted as S_M here, is determined by the intersection of the T–S curve representing the freezing point and that representing the isopycnal with density equal to that of the deep water. This criterion is shown as the vertical dashed line in Fig. 1. Using a deep-water density of $\rho = 1028\ \mathrm{kg\ m^{-3}}$, Malmberg (1969) derived $S_M = 34.7$ psu. Waters fresher than S_M freeze before getting dense enough to sink to the bottom. Given sufficient surface cooling, waters saltier than S_M can overturn, causing deep convection. This may help explain why deep convection capable of driving the global overturning cell occurs in the relatively salty North Atlantic and Antarctic but not in the fresher North Pacific, an issue returned to below.

However, several effects have been left out of this salinity criterion. First, there are location-specific effects like precipitation and freshwater runoff. These will be ignored here, as in Malmberg's (1969) analysis. Second, there are three other effects that can be dealt with more easily, at least to first order: 1) salinity increase through evaporation, 2) salinity increase through brine rejection during ice formation, and 3) salinity increase through entrainment of deep, saline water as the mixed layer deepens. The next three sections of this paper focus on how these effects modify Malmberg's criterion.

3. Modification of criterion for evaporation

a. Introduction

In the last section it was assumed that air–sea fluxes change the surface temperature but not the salinity. This is untrue if evaporation accompanies cooling, since evaporation increases the salinity of the seawater left behind. Figure 2 illustrates schematically how the combination of evaporation and cooling changes T–S trajectories. The criterion line (or curve, in the more general case) still emanates from the point of intersection of the deep-water isopycnal and the freezing point curve, as in Fig. 1, but now the local slope of the A and B trajectories is fixed by the ratio of evaporation and heat flux. (As stated above, additional effects such as precipitation and runoff can be accounted for in detailed local models but not here.) To determine this ratio, and thus the numerical form of the new temperature–salinity

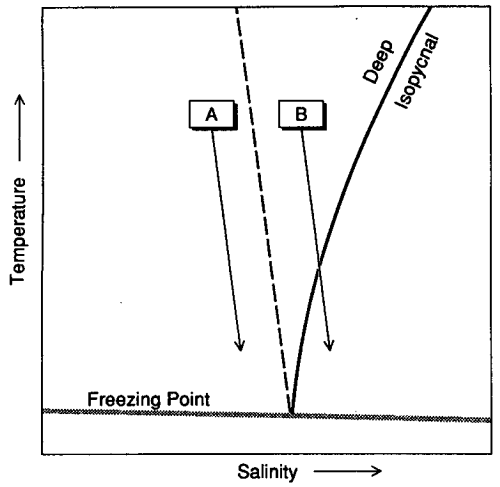

FIG. 2. Schematic T–S diagram illustrating the proposed T–S criterion allowing for evaporation at the sea surface. All symbols are as in Fig. 1, the only difference being that the trajectories A and B slope to the left by an amount determined by the air–sea flux laws. Surface waters to the right of the dashed line can take part in deep convection before ice forms. The dashed line thus demarks a temperature–salinity criterion, in analogy to Malmberg's (1969) salinity criterion of Fig. 1.

criterion, standard formulas for air–sea flux will be used.

b. *Flux formulas*

1) EVAPORATION

According to standard parameterizations of air–sea fluxes (Gill 1982), the evaporation rate E (kg m^{-2} s^{-1}) is proportional to the product of the wind speed U (m s^{-1}) and the difference in specific humidity $q = q(T, p)$ between the air at a standard level above the water surface (subscript a) and the saturated air near the water surface (subscript w):

$$E = \rho_a C_E U(q_w - q_a). \tag{1}$$

Here ρ_a is the air density and C_E is a dimensionless empirical coefficient. Gill (1982) recommends the use of 1.5×10^{-3} for C_E, and this value will be used in calculations here. (See Table 1, which lists all values used in calculations, together with references to the sources of the data.) Various studies have suggested C_E values that vary by 50%–100% from Gill's value (Friehe and Schmitt 1976; Liu et al. 1979; Smith 1988, 1989). Furthermore, individual data within studies typically have 50% scatter (Smith 1991; Katsaros and DeCosmo 1992). Whether C_E varies with wind speed is uncertain. Early work suggested that C_E varies by a factor of 2 over the relevant range of wind speeds (Smith 1989), but more recent measurements show no dependence on wind speed (Katsaros and DeCosmo 1992; Smith 1991). Bearing these facts in mind, an uncertainty of 50% will be assumed for C_E. This will translate to a similar percentage uncertainty in the slope of T–S trajectories of water masses.

The specific humidity q (unitless) is related to the partial pressure e (mb) of the water vapor through the intermediate formula

$$q = \frac{r}{1 + r}, \tag{2}$$

where the "mixing ratio" r (unitless) is given by (Iribarne and Godson 1981)

$$r = \frac{\epsilon e}{p - e}. \tag{3}$$

Here $\epsilon = 0.622$ is the ratio of the molecular weight of dry air to that of water vapor, and p (mb) is the atmospheric pressure. Since $p \approx 1000$ mb and $e < 10$ mb for the temperatures < 7 °C of interest here [see (5) below], (2) and (3) can be combined and approximated by

$$q \approx \frac{\epsilon e}{p} \tag{4}$$

without incurring an error exceeding 1%. Finally, q can be related to T and p by noting that e varies with temperature according to the Clausius–Clapeyron equation, which is approximated by the Magnus formula (Iribarne and Godson 1981) as

TABLE 1. Values used in calculations. In cases where a range of values is given, the central value is used in the calculations. Subscripts a, w, and i refer to air, water, and ice. Data sources are A: Iribarne and Godson (1981, Appendix 1), B: Gill (1982), C: Pounder (1965), D: Gill (1982), E: Gill (1982) (see also discussion in present text), F: Gill (1982) and Liu et al. (1979), G: value for dry air after Iribarne and Godson (1981, Appendix 1), H: Gill (1982, Appendix 3), I: Pounder (1965) for temperatures −2° to −20 °C, J: Weeks and Ackley (1986) (−2° to −20 °C), K: representative value used here, L: Iribarne and Godson (1981, Appendix 1), M: Ono (1967, Table 2) for −8° to −2°C and 7–12 psu, N: representative value used here, O: Iribarne and Godson (1981), and P: Cox and Weeks (1988) and Eicken (1992).

Item	Value	Unit	Source
ϵ	0.622	—	A
ρ_a	1.2 – 1.3	kg m^{-3}	B
ρ_i	910	kg m^{-3}	C
ρ_w	1028	kg m^{-3}	D
C_E	1.5×10^{-3}	—	E
C_H	$0.8 - 1.1(\times 10^{-3})$	—	F
c_{pa}	1000	J kg^{-1} °C^{-1}	G
c_{pw}	4000	J kg^{-1} °C^{-1}	H
k	2.3 – 2.5	W °C^{-1} m^{-1}	I
	2.1 – 2.3		J
	2.3 ± 0.2		K
L_f	3.3×10^6	J kg^{-1}	L
	$2.5 - 3.5 \times 10^6$		M
	$3.0 \pm 0.5 \times 10^6$		N
L_v	2.5×10^6	J kg^{-1}	O
S_i	4 – 9	psu	P

$$\log_{10} e = -\frac{2937.4}{T + T_0} - 4.9283 \log_{10}(T + T_0) + 23.547, \quad (5)$$

where $T_0 = 273.16°C$ converts from degrees Celsius to kelvin.

Taken together, (1), (4), and (5) yield the rate of evaporation, where $q_w = q(T_w, p)$ is calculated using the water temperature T_w and $q_a = q(T_a, p)$ is calculated using the air temperature T_a. Figure 3 shows $q = q(T, p)$ as a function of T at $p = 1000$ mb, illustrating that both q and dq/dT are much smaller at the low temperatures of cold-air outbreaks (Guest and Davidson 1991) than at the warm temperature of the saturated air near the warm water surface.

2) HEAT FLUX

Ignoring relatively small and location-specific contributions by solar insolation and longwave back radiation, the heat flux Q (W m^{-2}) out of the surface water is parameterized by

$$Q = \rho_a c_{pw} C_H U(T_w - T_a) + L_v E \quad (6)$$

(Gill 1982). In the first term, which represents the sensible heat flux, c_{pw} is the specific heat of seawater, U is the wind speed as above, and C_H is an empirically derived dimensionless coefficient. The second term represents cooling through evaporation, L_v being the latent heat of vaporization of water and E the evaporation rate as determined above.

c. *Predicted covariation of T and S*

Given these heat and water fluxes at the surface, and neglecting other sources and sinks, the depth-averaged temperature and salinity for a surface mixed layer of thickness H vary according to

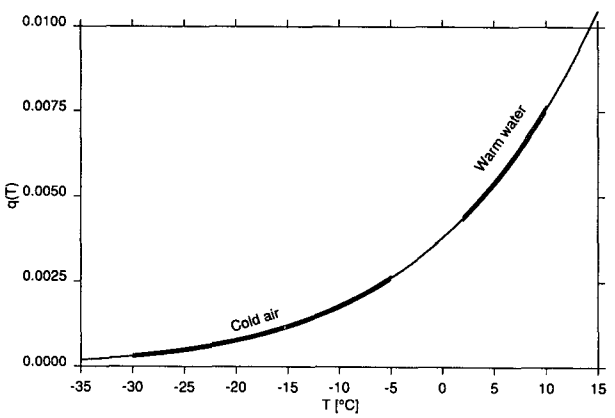

FIG. 3. Variation of specific humidity $q = q(T, p)$ as a function of temperature T, for a fixed pressure $p = 1000$ mb. (A reasonable range of pressures yields curves within a line width of the curve shown here.)

$$\frac{dT}{dt} = \frac{Q}{\rho_w c_{pw} H} \quad (7)$$

and

$$\frac{dS}{dt} = \frac{SE}{\rho_w H} \frac{1000}{1000 - S}, \quad (8)$$

where ρ_w is the water density. The fractional term containing the number 1000 converts S from practical salinity units into a mass fraction and will be neglected here for clarity, at the expense of a 3% error.

Combining (7) and the simplified form of (8) yields

$$\frac{dS}{dT} = \frac{c_{pw} E S}{Q}. \quad (9)$$

Note the lack of dependence on wind speed, since both flux components are proportional to wind speed. Using (1), (4), and (5) for the evaporation term and (6) for the heat flux term, (9) becomes

$$\frac{dS}{dT} = \frac{c_{pw} S}{L_v} \left(1 + \frac{c_{pw}}{L_v} \frac{C_H}{C_E} \frac{T_w - T_a}{q_w - q_a}\right)^{-1}. \quad (10)$$

Noting that specific humidity q depends on T alone, one infers that dS/dT depends only on air and water temperature. Figure 4 shows this dependence. The gray region indicates the range of T_a and T_w most likely to be found in regions of interest, such as the Labrador Sea, used as a test case in the next section. As noted above, uncertainties in C_E, C_H, etc., yield an uncertainty of perhaps 50% in dS/dT. The range in T_a and T_w yields a similar range in dS/dT. Roughly speaking, then, dS/dT is about 0.01 psu°C^{-1}, to within a factor of 2. Therefore, a seasonal temperature change of 10 °C can compensate a salinity difference of about 0.05–0.2 psu.

Simply stated, the result of accounting for evaporation is that Malmberg's salinity criterion $S_M = 34.7$ psu translates to a temperature–salinity criterion that allows salinities as low as 34.5 psu given the relevant seasonal temperature changes.

d. *Observed covariation of T and S in the Labrador Sea*

Through the 1960s and 1970s, hydrographic measurements were made approximately daily at Ocean Weather Station Bravo, located in the center of the entrance to the Labrador Sea at 56°N, 51°W. These long-term data provide a valuable insight into ocean variability in the North Atlantic (Smith and Dobson 1984; Lazier 1973, 1980). Here, we use the data for a more limited purpose: to provide a basis for testing the predicted covariation of T and S allowing for both cooling and evaporation. (Brine rejection is not an issue at this site, since the waters never get cold enough to freeze, and it will be shown in section 5 that

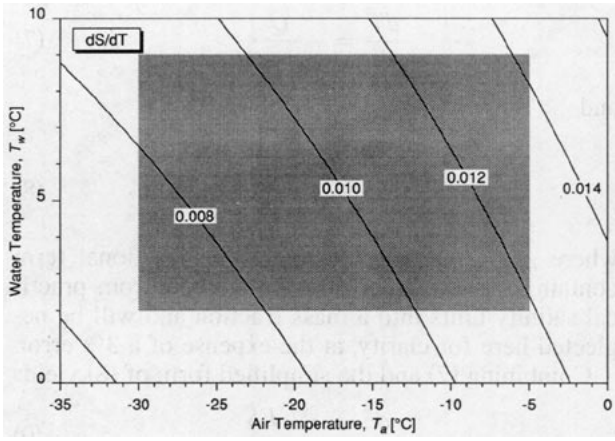

FIG. 4. Predicted inverse slope on T–S diagram, dS/dT (psu °C^{-1}), accounting for evaporation in addition to cooling, as a function of water temperature T_w and air temperature T_a. The shaded region indicates the relevant parameter range for the Labrador Sea.

at this site the effect of mixed-layer deepening is also fairly minor.) Since the arrival of the freshened waters of the "Great Salinity Anomaly" (Dickson et al. 1988) obscures the salinity signal greatly, only data for the years 1964 through 1967 will be used here. The data were linearly interpolated onto a uniform sampling interval (1 day) to allow digital filtering and were then low-pass filtered with a Butterworth filter having a half-power point of 100 days. This left a signal with slightly more information than a linear curve fit would have. Figure 5 shows the results, year by year, compared with the predicted covariation given by (10). The data were subsampled to show only the cooling months. The agreement in slope is generally good, given the year-to-year variability and the nearly factor of 2 uncertainty in the values of the parameters in (10).

4. Modification of criterion for brine rejection

Because the salinity of sea ice S_i is much less than that of seawater (Table 1), the brine rejected during freezing is saltier than the surrounding water. The resulting increase in surface salinity depends on the details of the mixing of the salty brine with surrounding waters (Rudels 1990; Wakatsuchi and Ono 1983). If, for simplicity, it is supposed that the brine mixes with a layer of thickness H, then the rate of increase of salinity in that layer will be

$$\frac{dS}{dt} = \frac{S - S_i}{H}\frac{dh}{dt}, \tag{11}$$

where h is the thickness of the ice formed. It has been assumed here for clarity of presentation that $h \ll H$; this is a reasonable assumption in most cases of interest, but it is easily relaxed. According to moored salinity observations in the Greenland Sea, dS/dt = 0.07–0.2 psu/mon (Roach et al. 1993). This monthly increase is comparable to the expected evaporative increase over several months (section 3), which suggests that the salinity increase may arise mostly from brine rejection in this basin. Equation (11) shows that two things determine changes in surface salinity: the rate of ice growth and the mixed layer depth. In specific geographical applications, these would normally be derived from a model driven by local atmospheric forcing and hydrography, but for the present purpose a simpler approach is appropriate. Supposing that H is given, the task is to estimate the ice growth rate dh/dt. The following crude analytical model is useful in highlighting parameter dependence of dh/dt. [Note that it is not promoted as a research tool in itself; in a numerical model, the process would normally be handled by integrating additional differential equations for snow and depth dependence within the ice (Semtner 1976; Lepparanta 1993).]

If the surface water is cooled to the freezing temperature, then the energy loss during further cooling will be at the expense of ice growth, so that

$$\rho_i L_f \frac{dh}{dt} = F, \tag{12}$$

where ρ_i is the density of ice, L_f is the latent heat of freezing, and F is the heat loss at the surface. The heat loss is given approximately by

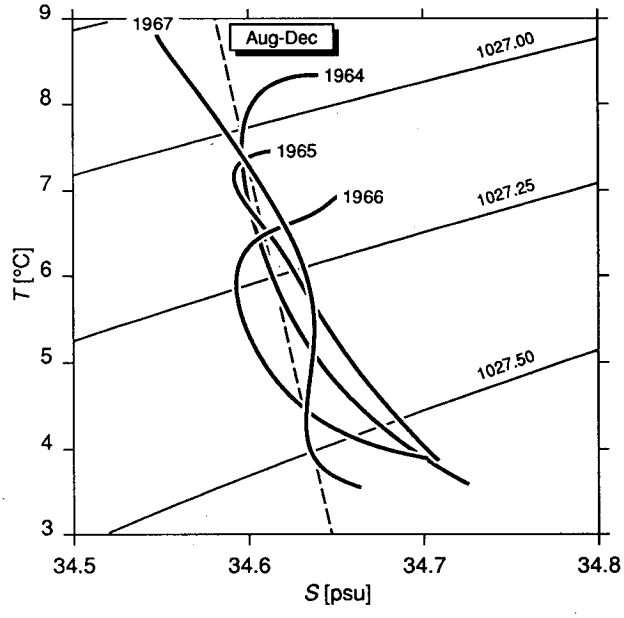

FIG. 5. Comparison of observed and predicted covariation of S and T at OWS Bravo in the Labrador Sea. The solid lines show the evolution of S and T from August to December in the indicated years. The raw data were first linearly interpolated to 25-m depth and then to daily values. A second-order Butterworth low-pass filter with cutoff at 100 days was then applied to smooth the curves, revealing the slope.

$$F = \rho_a c_{pa} C_H U (T_i - T_a), \tag{13}$$

where T_i is the temperature at the surface of the ice. Several terms have been left out of (13) for clarity. A relatively minor factor (as shown in section 5 below) is heat transport through entrainment of deep water as the mixed layer deepens due to convection driven by the brine rejection (Lepparanta 1993; Rudels 1990) and wind mixing. Two other missing terms express the rate of sensible and latent heat loss through leads (i.e., openings) in the ice. [For a review see Smith et al. (1990).] Roughly speaking, these terms can be subsumed into (13) by increasing the value of C_H. This is true because the sensible heat loss through leads is proportional to $(T_w - T_a)$, which is approximately equal to $(T_i - T_a)$, while the latent heat loss is proportional to $(q_w - q_a)$, which (since q_w is roughly linear in T_w and $q_a \ll q_w$ given the dryness of the air at the low temperatures of cold-air outbreaks) is also proportional to $(T_i - T_a)$.

If it is assumed that the ice provides a negligible insulating effect, perhaps if the open water areas transmit so much heat that the ice is an ineffective insulator over a given area, then T_i will equal the water temperature and will therefore be fixed at the freezing point T_f. For fixed T_a and U, the solution to (12) with (13) is

$$h = \frac{\rho_a c_{pa} U (T_f - T_a) t}{\rho_i L_f}. \tag{14}$$

Note that this has ice thickness growing linearly with time.

However, if the finite thermal conductivity of ice is taken into account, allowing for an insulating effect, then the temperature (T_i) at the top of the ice will be colder than that at the bottom (T_f), and the conductive flux through the ice, namely,

$$F_{cond} = k \frac{T_f - T_i}{h} \tag{15}$$

(where k is the thermal conductivity of sea ice), will equal the flux to the atmosphere. Thus,

$$\rho_a c_{pa} C_H U (T_a - T_i) = k \frac{T_i - T_f}{h} \tag{16}$$

so that the surface temperature is given by

$$T_i = (1 - f) T_f + f T_a, \tag{17}$$

where the nondimensional variable

$$f = \frac{\rho_a C_H c_{pa} h U}{k + \rho_a C_H c_{pa} h U} \tag{18}$$

has been isolated to express the degree of insulation provided by the ice. The parameter f is bounded between 0 and 1. The limit $f \to 1$ represents strong insulation, where the temperature at the ice surface approaches the air temperature. The limit $f \to 0$ corresponds to negligible insulation, so that surface of the ice is at the same temperature as the water below, that is, the freezing temperature T_f.

In the noninsulating $f \to 0$ limit, the above solution for no insulation is recovered, as expected. This limit is achieved if $k \gg \rho_a C_H c_{pa} h U$, or equivalently, if $h \ll h_0$, where $h_0 = k/(\rho_a C_H c_{pa})$ is a scale thickness. It is also achieved if leads (not modeled here) transmit much more heat than the ice. Using reasonable values of the parameters (Table 1), h_0 is calculated to be 0.2 m. Observations suggest that this thickness is achieved after a cooling of 50–100 degree-days (Anderson 1961).

In the insulating $f \to 1$ limit, using (17) in (15) allows the heat flux to be written

$$F = f k \frac{(T_f - T_a)}{h} \tag{19}$$

so that, using this in (12), one gets

$$h = \left(\frac{2k(T_f - T_a)t}{\rho_i L_f} \right)^{1/2}. \tag{20}$$

This is equivalent to the classical Stefan ice model [see Lepparanta's (1993) review]. Note that h varies as the square root of time, whereas in the conducting case the time dependence was linear. This qualitative difference is likely to be important in practice.

Leaving aside complicating factors such as leads and snow cover, we predict that ice thickness should increase linearly with time until a thickness h_0 is achieved and then increase in proportion to $t^{1/2}$ thereafter. This is borne out in field studies. Anderson (1961) has reported on a time series study of ice formation in a protected region where advection was unimportant. He summarizes his observations of ice growth with the following curve-fit formula

$$h^2 + 0.051h = 7.8 \times 10^{-9} \int (T_f - T_a) dt, \tag{21}$$

where the units of h are meters and the units of time t are seconds. The misfit between this curve and the observations is about 10%–20%. Thus, Anderson's measurements confirm the evolution of $h(t)$ predicted here, with initial linear growth giving way to square-root growth beyond an ice thickness of a fractional meter.

Anderson's empirical formula allows rough calculations to be made without calibrating analytical or numerical models for parameters such as k and L_f and without modeling leads. In the present application it provides a tool for predicting the rate of ice growth, and thus, using (11), the rate of salinity increase in the upper waters. For example, a cold-air outbreak with $T_a = -10\,^\circ\mathrm{C}$ (Guest and Davidson 1991), lasting for 2 days, will produce 0.08 m of ice and increase the salinity of the upper 100 m by 0.02 psu. Ten such

events would yield a salinity increase of 0.2 psu, comparable to the predicted evaporative increase over a whole season.

Thus, brine rejection is of comparable importance to evaporation in areas such as the Greenland Sea where ice formation is vigorous. Figure 6 shows a sketch of the combined evaporation plus brine rejection process in a schematic T–S diagram like those in Figs. 1 and 2. The trajectory is as in Fig. 2, except that if the surface water is cooled to the freezing point before deep convection ensues, then continued cooling will cause ice formation. Surface waters in thermodynamic equilibrium with the ice will increase in salinity while maintaining a temperature given by the freezing point expression $T = T_f(S)$. Graphically, the T–S locus for brine rejection water travels to the right along the freezing point curve (i.e., along arrow b in the figure). The relative lengths of the vectors labeled a and b in the figure depend on the salinity increase over a season, from evaporation and brine rejection. In this regard, Fig. 6 is drawn approximately to scale for the Greenland Sea, where brine rejection is probably an important aspect of deep convection. For ocean basins where creation of bottom water does not require ice formation (e.g., Mediterranean Sea, Labrador Sea), Fig. 2 is more relevant.

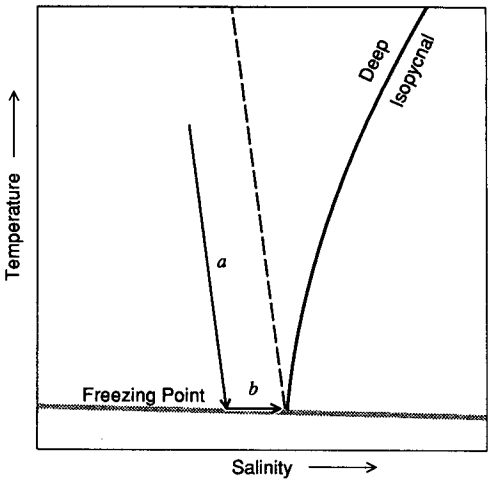

FIG. 6. Modification of criterion to account for brine rejection. The dashed line is the criterion neglecting brine rejection, as in Fig. 2. The arrows labeled a and b indicate T–S trajectories for cooling/evaporation followed by brine rejection. The length of arrow b is determined by the intensity and duration of ice formation, the line being drawn here at a scale roughly appropriate to the Greenland Sea. Waters to the right of the arrow labeled a are salty enough to convect to the density of the deep isopycnal.

5. Modification of criterion for mixed-layer deepening

As the mixed layer thickens because of convective and wind-driven mixing, the incorporation of deeper waters will alter the surface temperature and salinity. Although a mixed layer model, driven by air–sea fluxes of heat, water, and momentum, would be required to fully account for these effects (Pawlowicz et al. 1994), a rough estimate can be found by noting the observed mixed layer deepening rate and the temperature–salinity profiles of the region. For example, in the Labrador Sea, at the OWS Bravo site, the mixed layer deepens by ~50 m from August to December, and, given the background profiles of salinity and temperature, this should yield ~ 0.05–0.10 psu increase in salinity and a ~0.5°C decrease in temperature over these months. Figures 5 and 6 show that this temperature change is negligible compared to the observed (presumably atmospheric) cooling but that the salinity change is comparable to both the observed changes and the predicted effects of evaporation and brine rejection.

6. Discussion

Since the Greenland Sea is known to experience deep convection, it provides a good test case for the present discussion. The most basic question is whether the modifications to Malmberg's simpler criterion amount to a significant change, given realistic hydrography and forcing.

A preliminary answer is provided by Fig. 7, which shows a map of surface salinity in the convective region of the North Atlantic for the cooling months preceding the convective period. The data were objectively interpolated onto a 1° latitude/longitude grid by Levitus (1982). This grid resolution is inferior to that of individual ship transects, for example, those described by Worthington and Wright (1970), but the 3D space-filling nature of the Levitus data is more suited to the present mapping task. If the three Worthington and Wright (1970) transects near Greenland are taken as a reference, then use of the Levitus data yields ~70% underestimate of the salinity gradient.

The contours in Fig. 7 show the excess of S over Malmberg's (1969) critical value $S_M = 34.7$ psu. The waters near the coast are too fresh to convect, according to either Malmberg's criterion or the present criterion. Looking more closely, there are significant differences in the predictions of the two criteria. Taking a scale for autumn cooling of 10 °C, and with the observed rates of mixed layer deepening, the new T–S criterion yields a maximal allowed autumn salinity of S_M minus 0.3 psu (with no brine rejection) or 0.5 psu (with the addition of brine rejection at the rate observed in the Greenland Sea). The boundary line for the new criterion lies approximately along the $S_M - 0.5$ psu contour. The area between the boundary lines for the new and old criteria (i.e., the area with the thick contours in Fig. 7) is a large fraction of the

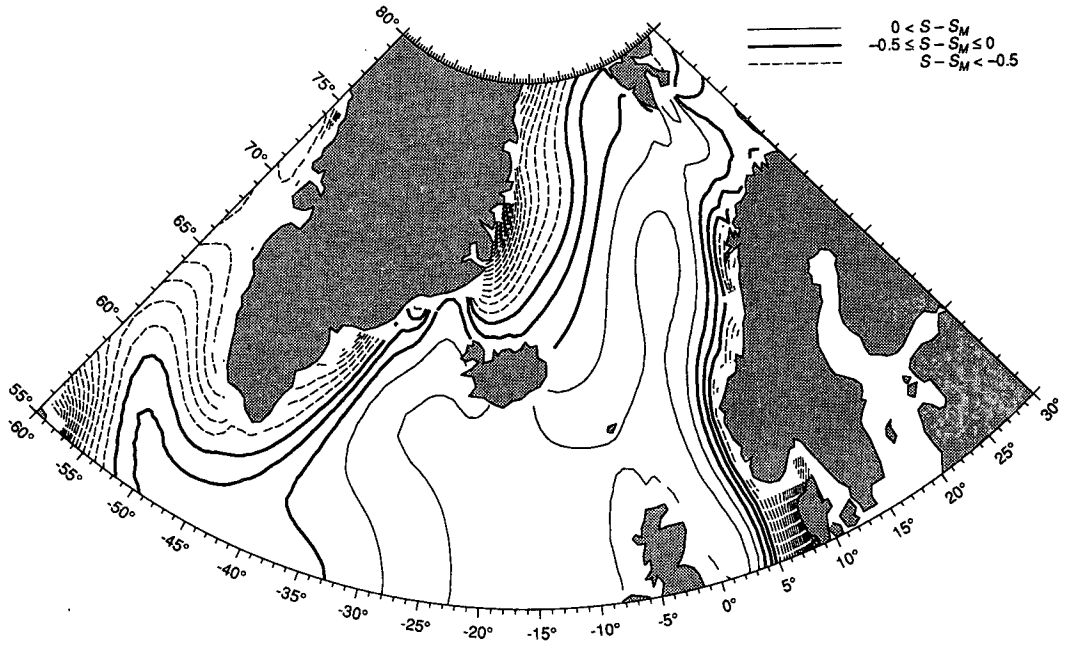

FIG. 7. Map of North Atlantic surface salinity from the Levitus (1982) atlas, showing the climatological average for November, December, and January. The contour interval is 0.25 psu, and the legend indicates the contour values. The dashed thin contour lines indicate areas where the surface waters are too fresh to convect. The solid thin contour lines indicate areas where the surface waters are salty enough to convect according to both the old and new criteria. The thick contour lines indicate areas where surface waters are convectively unstable (i.e., capable of replenishing the $\rho = 1028\,\mathrm{kg\,m^{-3}}$ isopycnal) according to the present criterion but not according to Malmberg's (1969) criterion. Note the large area that falls between the two criteria, especially near Greenland and in the Labrador Sea.

basin area, suggesting that the difference between the new and old criteria is important in this region. This is especially true in the Labrador Sea, a large area of which is predicted to be susceptable to deep convection by the new criterion. The new boundary line is 100–200 km closer to the continent of Greenland than the old boundary line. [If the Levitus data are oversmoothed, as the Worthington and Wright (1970) atlas suggests, this offset is overestimated by 70% for the Greenland Sea, but the result is little changed for the Labrador Sea, where the area between the two criteria is much larger.] This is significant since the forcing for deep convection is likely to be cold air outbreaks from the continent (Guest and Davidson 1991), which yield a buoyancy flux that decays in the offshore direction as the air warms and humidifies while blowing over the water. Thus, the onshore displacement of the predicted convection boundary implies that the potentially convective water will experience increased buoyancy loss to the atmosphere. Seung (1987) calculates the offshore scale for reduction of the buoyancy flux to be a few hundred kilometers. Since the onshore shift of the stability boundary is similar to this offshore folding decay scale of buoyancy flux, it is evident that the new and old criteria make significantly different predictions about deep convection in the North Atlantic.

On a global scale, the criteria are not so different as they are in the North Atlantic. Figure 8 shows the surface salinity map for the North Pacific. Here the salinities are 2–3 psu less than the critical value, which suggests that these waters are so fresh that convection capable of refreshing the $1028\,\mathrm{kg\,m^{-3}}$ isopycnal is not permitted, either by Malmberg's (1969) criterion or the present criterion [although shallower convection is of course possible; see Van Scoy et al. (1991) and Van Scoy and Druffel (1993)]. Thus, both criteria agree in their explanation of the observed lack of globally significant deep convection in North Pacific.

7. Summary and conclusions

Malmberg's (1969) salinity criterion for the inhibition of deep convection was extended here to account for the increase of salinity associated with evaporative cooling, brine rejection, and mixed-layer deepening. Standard air–sea flux formulas were used to calculate the effect of evaporation. As a preliminary step, the predicted coevolution of T and S was checked using a decadal time series of hydrography in the Labrador Sea (where brine rejection is less significant than in the Greenland Sea). The agreement was within error estimates. The new criterion allowing for evap-

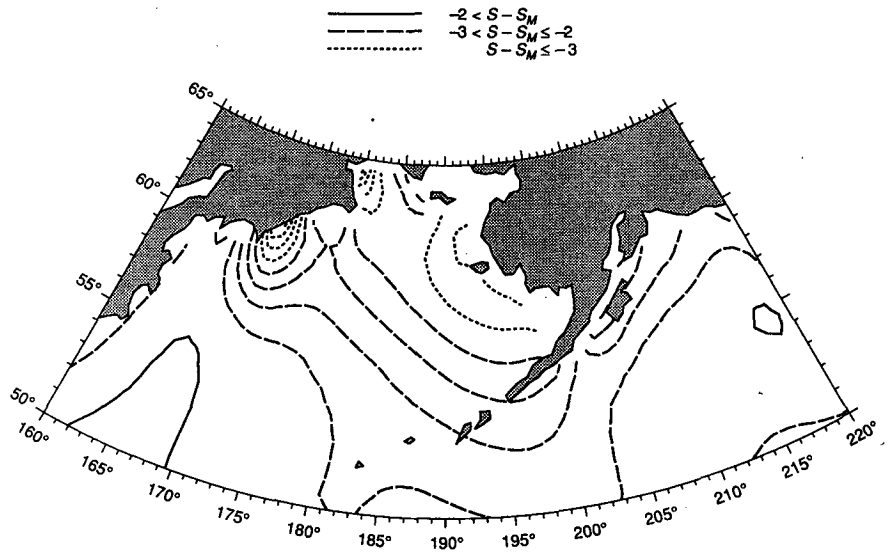

FIG. 8. As in Fig. 7 except for the North Pacific. As the legend indicates, all waters here are too fresh to convect deeply enough to replenish the $\rho = 1028\,\mathrm{kg\,m^{-3}}$ isopycnal.

oration is similar to the old salinity criterion, except that it is represented by a sloped line in a temperature–salinity diagram. Given typical seasonal cooling rates, this permits deep convection in waters up to 0.2 psu fresher than Malmberg's criterion. Adding the salinizing effect of brine rejection offsets the sloped line toward lower salinity by an amount dependent on the mixed layer depth and the amount of ice formation. This term is about 0.2 psu in the Greenland Sea. The effect of mixed layer deepening is to allow an additional 0.1 psu. Taking these effects together, the new criterion allows convection in water up to about 0.5 psu fresher than Malmberg's criterion.

On the global scale, the old and new criteria agree in predicting that the North Pacific Ocean is too fresh to drive the observed global overturning cell and that the North Atlantic Ocean is salty enough.

Locally, the difference between the old and new criteria is quite significant. Maps of the salinity anomaly in the North Atlantic were presented to illustrate the geographical location of the boundary between relatively fresh inshore water and the saltier offshore water, capable of being cooled and salinized enough to cause deep convection. Using the new criterion moves this boundary inshore by several hundred kilometers, a significant fact for two reasons. First, the area between the two boundaries is a sizeable fraction of local basin geometry, which means that the geographical regions susceptible to deep convection are significantly enlarged. Second, the inshore movement of the boundary effectively puts the potentially convective water nearer the region of strongest atmospheric forcing. In fact, the onshore offset of the boundary is the same as the offshore decay scale of heat flux in the continental cold-air outbreaks that drive deep convection, suggesting that the effects considered here may be important at first order.

Acknowledgments. This work was supported by an NSERC operating grant and by an NSERC WOCE special collaborative grant. I thank Sydney Levitus for providing his climatological data for the Greenland Sea, and John Lazier for providing the OWS Bravo dataset of Labrador Sea measurements. I also thank Eric Kunze for comments on the manuscript, and the two anonymous referees for their useful suggestions.

REFERENCES

Anderson, D. L., 1961: Growth rate of sea ice. *J. Glaciol.*, **3,** 1170–1172.

Boyle, E. A., 1990: Quaternary deepwater paleoceanography. *Science,* **249,** 863–870.

Brewer, P. G., W. S. Broecker, P. B. Rhines, C. G. Rooth, J. H. Swift, T. Takahashi, and R. T. Williams, 1983: A climatic freshening of the deep Atlantic north of 50°N over the past 20 years. *Science,* **222,** 1237–1239.

Broecker, W. S., 1975: Climatic change: Are we on the brink of a pronounced global warming? *Science,* **189,** 460–463.

——, 1991: The great ocean conveyor. *Oceanography,* **4,** 79–89.

——, 1992: Global warming on trial. *Natural History,* April, 6–14.

——, and G. H. Denton, 1989: The role of ocean-atmosphere reorganizations in glacial cycles. *Geochim. Cosmochim. Acta,* **53,** 2465–2501.

Cox, C. F. N., and W. F. Weeks, 1988: Numerical simulations of the profile properties of undeformed first-year sea ice during the growth season. *J. Geophys. Res.,* **93,** 12 449–12 460.

Dickson, R. R., J. Meincke, S.-A. Malmberg, and A. J. Lee, 1988: The "Great Salinity Anomaly" in the northern North Atlantic, 1968–1982. *Progress in Oceanography,* Vol. 20, Pergamon, 103–151.

Eicken, H., 1992: Salinity profiles of Antarctic sea ice: Field data and model results. *J. Geophys. Res.,* **97,** 15 545–15 557.

Friehe, C. A., and K. F. Schmitt, 1976: Parameterization of air-sea interface fluxes of sensible heat and moisture by bulk aerodynamic formulas. *J. Phys. Oceanogr.*, **6,** 801–809.

Gill, A. E., 1982: *Atmosphere–Ocean Dynamics.* Academic Press, 662 pp.

Guest, P. S., and K. L. Davidson, 1991: Meteorological triggers for deep convection in the Greenland Sea. *Deep Convection and Deep Water Formation in the Oceans,* Elsevier, 382 pp.

Hakkinen, S., G. L. Mellor, and L. H. Kantha, 1992: Modeling deep convection in the Greenland Sea. *J. Geophys. Res.*, **97,** 5389–5408.

Iribarne, J. V., and W. L. Godson, 1981: *Atmospheric Thermodynamics.* Reidel, 259 pp.

Katsaros, K. B., and J. DeCosmo, 1992: Water vapor flux from the sea at high wind speeds. *Int. Symp. on Tropical Cyclone Disasters,* Beijing, China, ICSU/WMO.

Keigwin, L. D., G. A. Jones, S. J. Lehman, and E. A. Boyle, 1991: Deglacial meltwater discharge, North Atlantic deep circulation, and abrupt climate change. *J. Geophys. Res.*, **96,** 16 811–16 826.

Lazier, J. R. N., 1973: The renewal of Labrador Sea Water. *Deep-Sea Res.*, **20,** 341–353.

——, 1980: Oceanographic conditions at Ocean Weather Ship Bravo, 1964–1974. *Atmos.-Ocean,* **18,** 227–238.

Lepparanta, M., 1993: A review of analytical models of sea-ice growth. *Atmos.-Ocean,* **31,** 123–138.

Levitus, S., 1982: *Climatological Atlas of the World Ocean.* NOAA Prof. Paper No. 13, 173 pp.

——, 1989: Interpentadal variability of temperature and salinity in the deep North Atlantic, 1970–1974 versus 1955–1959. *J. Geophys. Res.*, **94,** 16 125–16 132.

——, 1990: Interpentadal variability of steric sea level and geopotential thickness of the North Atlantic ocean, 1970–1974 versus 1955–1959. *J. Geophys. Res.*, **95,** 5233–5238.

Liu, W. T., K. B. Katsaros, and J. A. Businger, 1979: Bulk parameterization of air-sea exchanges of heat and water vapor including the molecular constraints at the interface. *J. Atmos. Sci.*, **36,** 1722–1735.

Madec, G., M. Chartier, and M. Crepon, 1991a: The effect of thermohaline forcing variability on deep water formation in the western Mediterranean Sea: A high-resolution three-dimensional numerical study. *Dyn. Atmos. Ocean,* **15,** 301–332.

——, P. Delecluse, and M. Crepon, 1991b: A three-dimensional numerical study of deep-water formation in the northwestern Mediterranean Sea. *J. Phys. Oceanogr.*, **21,** 1349–1371.

Malmberg, S.-A., 1969: Hydrographic changes in the waters between Iceland and Jan Mayen in the last decade. *Jökull,* **19,** 30–43.

Marsden, R. F., L. A. Mysak, and R. A. Myers, 1991: Evidence for stability enhancement of sea ice in the Greenland and Labrador seas. *J. Geophys. Res.*, **96,** 4783–4789.

Mysak, L. A., D. K. Manak, and R. F. Marsden, 1990: Sea-ice anomalies observed in the Greenland and Labrador seas during 1901–1984 and their relation to an interdecadal Arctic climate cycle. *Climate Dyn.*, **5,** 111–133.

Ono, N., 1967: Specific heat and heat of fusion of sea ice. *Physics of Snow and Ice,* Institute of Low Temperature Science, Hokkaido University, 1414 pp.

Pawlowicz, R., J. F. Lynch, W. B. Owens, P. F. Worcester, W. M. L. Morawitz, and P. J. Sutton, 1994: Thermal evolution of the Greenland Sea gyre in 1988-1989. *J. Geophys. Res.*, submitted.

Pounder, E. R., 1965: *The Physics of Ice.* Pergamon, 151 pp.

Read, J. F., and W. J. Gould, 1992: Cooling and freshening of the subpolar North Atlantic Ocean since the 1960s. *Nature,* **360,** 55–57.

Roach, A. T., K. Aagaard, and F. Carsey, 1993: Coupled ice-ocean variability in the Greenland Sea. *Atmos.-Ocean,* **31,** 319–337.

Rooth, C., 1982: Hydrology and ocean circulation. *Progress in Oceanography,* Vol. 11, Pergamon, 131–149.

Rudels, B., 1990: Haline convection in the Greenland Sea. *Deep-Sea Res.*, **37,** 1491–1511.

Schlosser, P., G. Bonisch, M. Rhein, and R. Bayer, 1991: Reduction of deepwater formation in the Greenland Sea during the 1980s: Evidence from tracer data. *Science,* **251,** 1054–1056.

Semtner, A. J., 1976: A model for the thermodynamic growth of sea ice in numerical investigations of climate. *J. Phys. Oceanogr.,* **6,** 379–389.

Seung, Y.-H., 1987: A buoyancy flux-driven cyclonic gyre in the Labrador Sea. *J. Phys. Oceanogr.,* **17,** 134–146.

Skyllingstad, E. D., D. W. Denbo, and J. Downing, 1991: Convection in the Labrador Sea: Community modeling effort (CME) results. *Deep Convection and Deep Water Formation in the Oceans,* Elsevier, 382 pp.

Smith, S. D., 1988: Coefficients for sea surface wind stress, heat flux, and wind profiles as a function of wind speed and temperature. *J. Geophys. Res.*, **93,** 15 467–15 472.

——, 1989: Water vapor flux at the sea surface. *Bound.-Layer Meteor.,* **47,** 277–293.

——, 1991: Some early results of the humidity exchange over the sea main experiment. *Deep Convection and Deep Water Formation in the Oceans,* Elsevier, 382 pp.

——, and F. W. Dobson, 1984: The heat budget at ocean weather station Bravo. *Atmos.-Ocean,* **22,** 1–22.

——, R. D. Muench, and C. H. Pease, 1990: Polynyas and leads: An overview of physical processes and environment. *J. Geophys. Res.*, **95,** 9461–9479.

Van Scoy, K. A., and E. R. M. Druffel, 1993: Ventilation and transport of thermocline and intermediate waters in the North Pacific during recent El Ninos. *J. Geophys. Res.*, **98,** 18 083–18 088.

——, D. B. Olson, and R. A. Fine, 1991: Ventilation of North Pacific intermediate waters: The role of the Alaskan gyre. *J. Geophys. Res.*, **96,** 16 801–16 810.

Wakatsuchi, M., and N. Ono, 1983: Measurements of salinity and volume of brine excluded from growing sea ice. *J. Geophys. Res.*, **88,** 2943–2951.

Weaver, A. J., and T. M. C. Hughes, 1992: Stability and variability of the thermohaline circulation and its link to climate. *Trends in Physical Oceanography,* Council of Sci. Res. Integration, 15–70.

Weeks, W. F., and S. F. Ackley, 1986: The growth, structure, and properties of sea ice. *The Geophysics of Sea Ice,* 1196 pp.

Worthington, L. V., and W. R. Wright, 1970: *North Atlantic Ocean Atlas.* Woods Hole Oceanographic Institution, 24 pp.

Wright, D. G., and T. F. Stocker, 1993: Younger Dryas experiments. *Ice in the Climate System,* W. R. Peltier, Ed., Springer-Verlag, 395–416.